Available online at www.sciencedirect.com

ScienceDirect

journal homepage: www.elsevier.com/locate/he

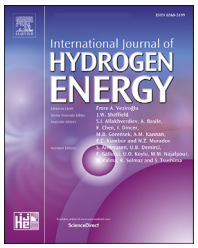

Neutron scattering study of tantalum monohydride and monodeuteride

Mikhail A. Kuzovnikov [a,*], *Vladimir E. Antonov* [a], *Alexandre S. Ivanov* [b], *Thomas Hansen* [b], *Stanislav Savvin* [b], *Valery I. Kulakov* [a], *Marek Tkacz* [c], *Alexander I. Kolesnikov* [d]

[a] *Institute of Solid State Physics RAS, 142432, Chernogolovka, Moscow, Russia*
[b] *Institut Laue-Langevin, 71 Avenue des Martyrs CS 20156, 38042, Grenoble Cedex 9, France*
[c] *Institute of Physical Chemistry PAS, 44/52 Kasprzaka, 01-224, Warsaw, Poland*
[d] *Neutron Scattering Division, Oak Ridge National Laboratory, Oak Ridge, TN, 37831, USA*

HIGHLIGHTS

- Tantalum monohydride and monodeuteride are synthesized
- Their full crystal structures are solved
- Their vibrational spectra are measured

ARTICLE INFO

Article history:
Received 19 January 2021
Received in revised form
18 March 2021
Accepted 19 March 2021
Available online 16 April 2021

Keywords:
Hydrogen storage materials
Crystal structure
Phonons
High-pressure
Neutron diffraction
Inelastic neutron scattering

ABSTRACT

Powder samples of $TaH_{0.89}$ and $TaD_{0.96}$ are synthesized under a hydrogen (deuterium) pressure of 2.8 GPa and a temperature of 250 °C, then quenched to the liquid nitrogen temperature, recovered to ambient pressure and studied by neutron diffraction (ND) and inelastic neutron scattering (INS). The ND study shows that both hydrogen and deuterium atoms occupy tetrahedral interstitial sites in a distorted body centered cubic (*bcc*) crystal structure of metal atoms, while the ordering scenarios in $TaH_{0.89}$ and $TaD_{0.96}$ are different. Hydrogen and deuterium atoms are ordered in a layered fashion, forming long period superstructures with space groups $P\bar{4}$ and $P222$, respectively, so that the unit cells of the crystal structures of $TaH_{0.89}$ and $TaD_{0.96}$ are $\sqrt{2} \times \sqrt{2} \times 7$ and $\sqrt{2} \times \sqrt{2} \times 8$ supercells of the initial cubic unit cell. The INS study demonstrates a pronounced "soft" (trumpet-like) anharmonicity of the potential well for H and D atoms.

Introduction

Metal hydrides are widely used for hydrogen and energy storage, and a proper understanding of metal-hydrogen interactions is important for designing new materials with advanced properties. The fundamental properties of hydrides are dominated by the high-frequency vibrations of hydrogen atoms, which are responsible for unusual phenomena, such as nearly room-temperature superconductivity, recently

* *Corresponding author.*
E-mail address: kuz@issp.ac.ru (M.A. Kuzovnikov).
https://doi.org/10.1016/j.ijhydene.2021.03.149

found at 203 K in body centered cubic (*bcc*) H_3S [1,2], at ~220 K in *bcc*-YH_6 [3,4], at 243 K in hexagonal close packed (*hcp*) YH_9 [4], and at 250 K in face centered cubic (*fcc*) LaH_{10} [5,6].

Although numerous new binary hydrides were discovered in recent years, the full crystal structure of only one of them, *hcp*-TaH_2, was determined [7].

Hydrogen interaction with group V transition metals vanadium, niobium and tantalum with *bcc* crystal structure has been studied for a long time [8,9]. The V–H, Nb–H and Ta–H systems are unique among other metal-hydrogen systems because of their high complexity, and because of high mobility of hydrogen atoms in these metals, which ensures that the thermodynamical equilibrium is quickly established at room temperature and above. This makes these systems good model objects for studying metal-hydrogen interactions, both experimentally and theoretically. Hydrogen forms a continuous interstitial solid solution in the *bcc* lattice of these metals at temperatures above 200 °C and concentrations up to H/Me = 1. At lower temperatures and 0 < H/Me < 1, these systems demonstrate extreme complexity due to the presence of multiple phases with slightly distorted *bcc* metal lattice, which differ from each other in the ordering of hydrogen atoms. Hydrogen and deuterium atoms invariably occupy tetrahedral interstitial sites, or T-sites, in all low-temperature phases in the Nb–H(D) and Ta–H(D) systems, and, additionally, octahedral interstitial sites, or O-sites, can be occupied in some of the VH_x and VD_x phases.

The phase diagrams of the V–H and V-D systems significantly differ from each other [9,10]. Among all studied Me-D systems, only the V-D and La-D [5] systems demonstrate phases with composition and crystal structure different from that in the Me–H counterparts. In the V–H(D) case, this is a result of a close competition of H(D) atom energies at the T- and O-sites. An important contribution to this energy comes from zero-point energy of the H(D) vibrations, which is different for the T- and O-sites.

A detailed review of the V–H(D), Nb–H(D) and Ta–H(D) systems at 0 < H(D)/Me < 1 is given in Ref. [9]. In the low-temperature limit, there are 3 presently known phases in the phase diagram of the Ta–H(D) system, whose crystal structures were established by neutron diffraction. These are Ta_2D [11], $Ta_3H(D)_2$ [12], and Ta_4D_3 [13,14]. The crystal structures of these phases are based on the $\sqrt{2}\times\sqrt{2}\times 1$, $4\sqrt{2}\times 3\sqrt{2}\times 1$ and $2\sqrt{2}\times\sqrt{2}\times 1$ supercells of the original *bcc* cell, respectively. Additionally, there are two phases with tentative compositions $TaH_{\sim 0.8}$ [15] and $TaH_{\sim 0.85}$ [16] with unknown crystal structures. Until now, tantalum hydrides with 0 < H/Ta < 1 have not been considered in *ab initio* calculations [17].

The vibrational properties of hydrogen (deuterium) solutions in tantalum were studied by INS in $TaH_{0.037}$, $TaH_{0.18}$ [18], $TaD_{0.22}$ [19] $TaH_{0.1}$ [20], $TaH_{0.08}$, $TaD_{0.14}$ [21], and $TaH_{0.71}$ [22]. The fundamental band of hydrogen vibrations in these tantalum hydrides consists of two peaks. The peak at 114–130 meV corresponds to a vibration in a direction to the nearest O-site, and the peak at 154–170 meV is caused by a nearly double degenerate vibration in the perpendicular

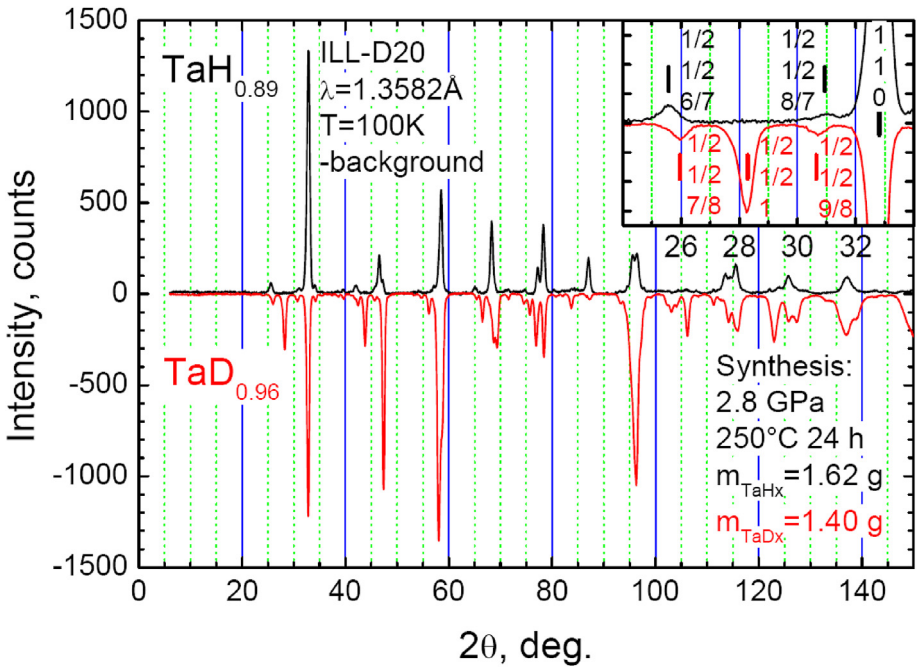

Fig. 1 – Neutron powder diffraction patterns of the $TaH_{0.89}$ (black curve) and $TaD_{0.96}$ (red curve) samples measured at $T = 100$ K with the D20 diffractometer at ILL. A smooth background was subtracted from both patterns, and the intensity axis was inverted for $TaD_{0.96}$. The inset shows a magnified view of the superstructural reflections at 2θ ~30° indexed in the *bcc* axes. Note that the $(^1/_2, ^1/_2, 1)_{bcc}$ superstructure peak at about 28.2° is clearly visible in the deuteride, but is absent in the hydride. (For interpretation of the references to color in this figure legend, the reader is referred to the Web version of this article.)

plane. The frequency ratio of the H and D fundamentals was found to be $E(H)/E(D) \approx 1.38$ for low H(D) concentrations [19,21]. The first harmonic of the lower fundamental H vibration in tantalum is anharmonically shifted to lower energies by about 15 meV [21,22], and this shift is about 9 meV for the D atom vibrations [21].

Under the hydrogen pressure of few bars, vanadium and niobium form dihydrides with *fcc* metal lattice and hydrogen atoms at the T-sites. Under the hydrogen pressure of several tens of GPa, niobium forms a series of new hydrides, such as *hcp*-NbH_2, double hexagonal close-packed $NbH_{2.5}$, and cubic *cI*16-NbH_3 [23]. Until recently, the maximal hydrogen solubility ever observed in tantalum only reached H/Ta = 0.86 at 1.6 GPa and 400 K [24]. The concentration range H(D)/Ta = 0.86–1 has not been studied in detail previously, because the synthesis of the samples required high pressures. Thanks to the development of methods of compressing molecular hydrogen in diamond anvil cells (DAC) two new tantalum hydrides were discovered at higher pressures – *hcp*-$TaH_{2.2}$ at 2.2 GPa [25] and *cI*16-TaH_3 at 42 GPa [26]. Neutron diffraction study of *hcp*-$TaH_{2.2}$ has shown that hydrogen atoms occupy both T- and O-sites, and inelastic neutron scattering demonstrated that the potential well for H atom is strongly anharmonic at both T- and O-sites [7].

In the present paper, we achieved the maximal hydrogen and deuterium solubility in *bcc* tantalum before its conversion to the *hcp* dihydride. Powder samples of $TaH_{0.89}$ and $TaD_{0.96}$ were synthesized under a hydrogen (deuterium) pressure of 2.8 GPa and a temperature of 250 °C and studied with ND and INS. Surprisingly, despite the identical synthesis routes and similar compositions, the H and D ordering scenarios turned out to be different. The vibrational properties of both H and D atoms in Ta demonstrated strong trumpet-like anharmonicity.

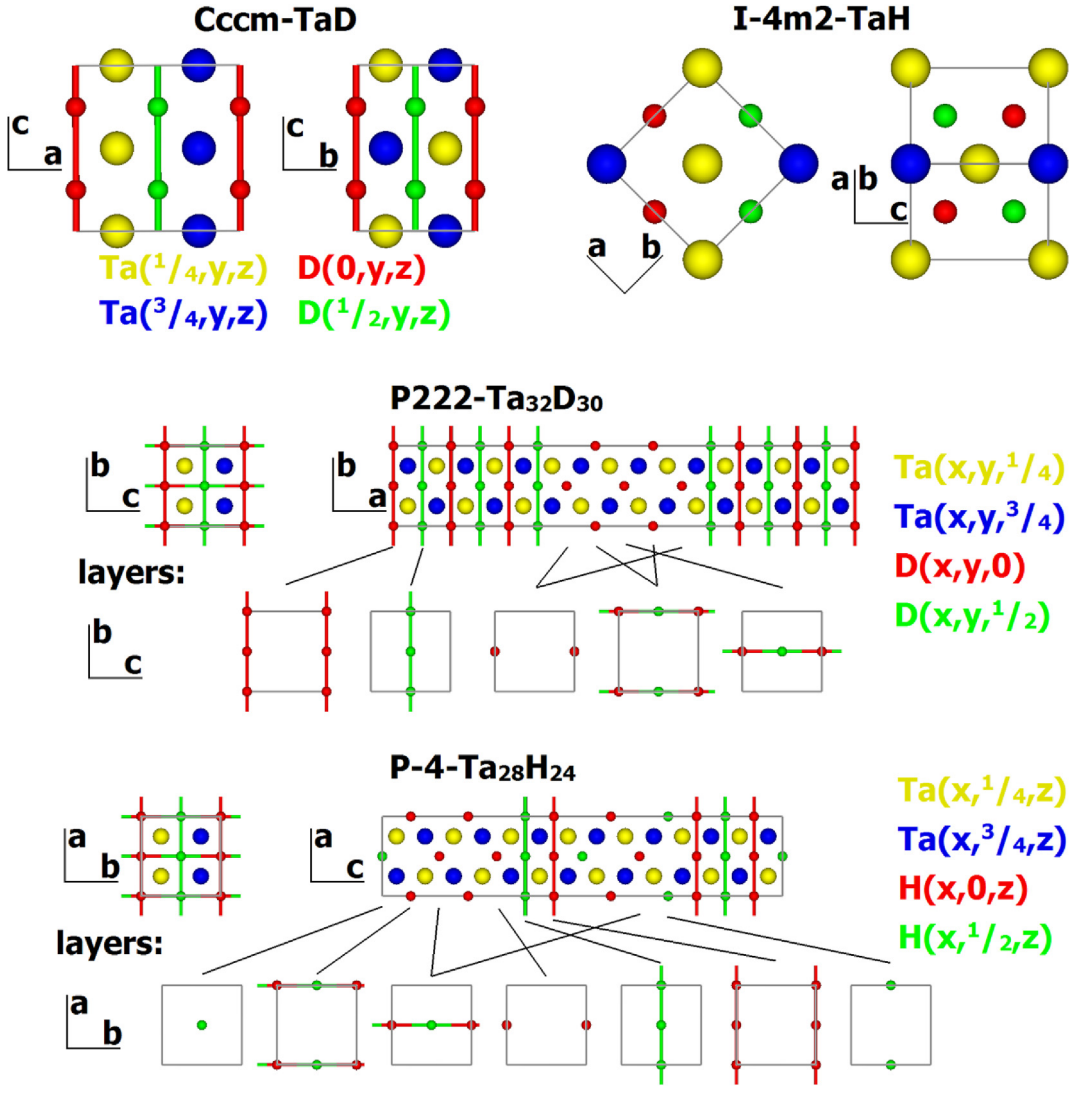

Fig. 2 – Model crystal structures of TaH and TaD used in the Rietveld refinement of the obtained ND patterns. The colored lines show the shortest H–H (D–D) distances, which in all cases are about 2.40 Å. The bcc unit cell of the $I\bar{4}m2$-TaH phase is rotated by 45° to keep the same alignment of the host *bcc* lattice of Ta atoms in all phases.

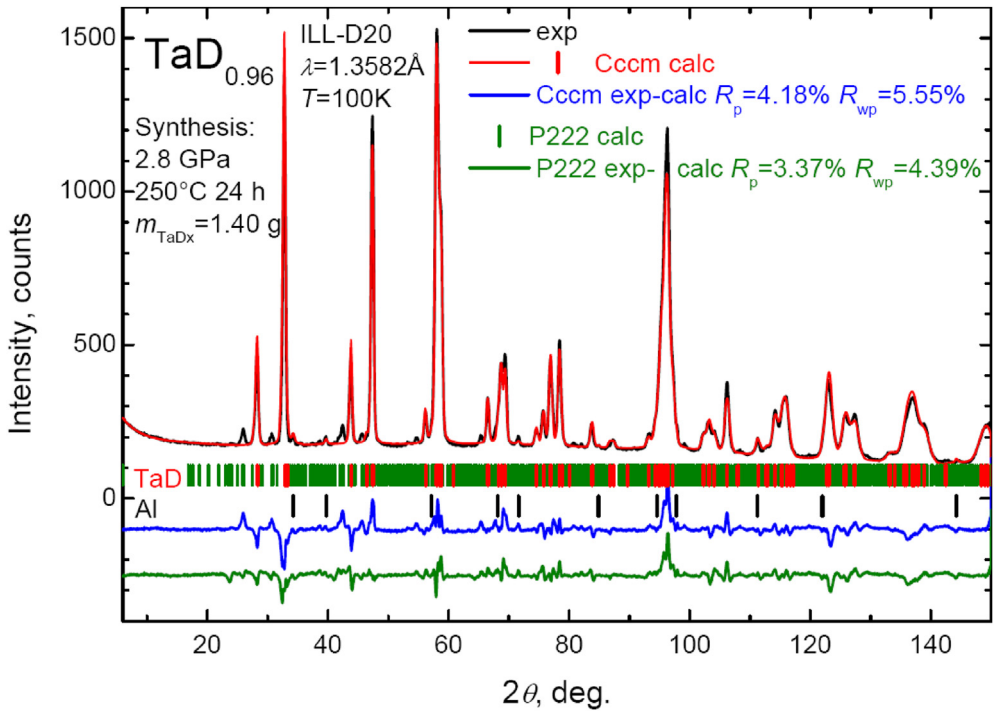

Fig. 3 – Neutron powder diffraction pattern of the $TaD_{0.96}$ sample (black curve) measured at $T = 100$ K with the D20 instrument at ILL, and the results of its Rietveld analysis using the *Cccm* and *P222* structural models. The refined structural parameters are listed in Tables 1 and 2, respectively.

Table 1 – Structural parameters obtained from the Rietveld refinement of the NPD pattern of $TaD_{0.96}$ using the *Cccm* (#66) model. The lattice parameters are $a = 4.792(1)$ Å, $b = 3.472(1)$ Å, and $c = 4.833(1)$ Å. The refinement residual is shown by the blue curve at the bottom of Fig. 3; the reliability factors are $R_p = 4.18\%$ and $R_{wp} = 5.55\%$. The atomic displacement parameter U_{iso} for the Ta atoms was fixed at zero, because its inclusion in the refinement did not improve the reliability factors.

Atom	Wyckoff position	x	y	z	U_{iso}, Å^2	w
Ta	4e	1/4	1/4	0	0	1
D	4a	0	0	1/4	0.008(1)	0.69(1)

Material and methods

The single-phase powder samples of tantalum hydride and deuteride with the total mass of 1.62 g and 1.40 g were synthesized using the same method as in our previous works [7,25]. The plates of a 99.9% Ta foil with a thickness of 0.16 mm were loaded with hydrogen (deuterium) by a 24 h exposure to an $H(D)_2$ atm at 2.8 GPa and 250 °C in a Lentil-type high-pressure chamber [27] using AlH_3 or AlD_3 as internal hydrogen (deuterium) source [28]. The protium contamination in the initial AlD_3 was $H/(H + D) = 1.5 \pm 0.5\%$ according to the spectral analysis. After the hydrogenation was completed, the samples were cooled together with the chamber to the liquid N_2 temperature; the pressure was released; the chamber was disassembled under liquid nitrogen; the samples were recovered from the chamber and further stored in liquid nitrogen in order to prevent H(D) losses.

Each sample was then examined by X-ray diffraction at 85 K to ensure that it was single-phase. The samples had compositions H/Ta = 0.89(3) and (D + H)/Ta = 0.96(3) as determined by hot extraction into a pre-evacuated volume. The hot extraction method is described elsewhere [25]. It was not possible to produce stoichiometric samples TaH or TaD by simply increasing the synthesis pressure because of the formation of, respectively, *hcp* tantalum dihydride or dideuteride [25]. Thus, our samples had the maximal H(D) saturation achievable on the basis of the *bcc* crystal structure of Ta atoms. For brevity, the present samples will be referred to as TaH and TaD. Before the neutron scattering experiments the samples were ground in an agate mortar under liquid nitrogen to reduce texture effects.

The powder samples thus prepared were studied by neutron diffraction at $T = 100$ K with the high-luminosity D20 diffractometer [29] at the Institute Laue-Langevin in Grenoble [30]. The data acquisition time was 2 h for each sample. Rietveld refinements were done with the FULLPROF 7.00 program [31]. Neutron wavelength and detector zero-shifts were determined from a Rietveld analysis of the diffraction pattern of a $Na_2Ca_3Al_2F_{14}$ standard measured separately.

Inelastic neutron scattering was studied on the same samples at $T = 10$ K with the IN1-Lagrange inverted geometry spectrometer [32] installed at the hot source of the high-flux reactor at ILL [33]. A background from the cryostat without the samples, but with the sample holder made of aluminium foil and the water ice condensed on it while loading, was measured separately under the same conditions and

subtracted from the experimental INS spectra. The resulting spectra were normalized to the constant neutron flux at the sample. Further details on neutron scattering experiments are given elsewhere [7].

Results and discussion

Neutron diffraction

The neutron powder diffraction patterns of our TaH and TaD samples are compared in Fig. 1. Apart from the usual system of *bcc* reflections with minor splitting, common for both samples, two different complex systems of superstructural reflections are observed for TaH and TaD. These reflections could not be explained by the presence of low-temperature $Ta_2H(D)$ [11], $Ta_3H(D)_2$ [12], or $Ta_4H(D)_3$ [13,14] phases, which are presently known in the Ta–H(D) system at $0 < H(D)/Ta < 1$.

TaD

Many years ago, a low-resolution neutron diffraction investigation of a $TaD_{0.87}$ sample showed that its crystal structure was orthorhombic and belonged to the space group *Cccm*, $a \approx c \approx a_{bcc}\sqrt{2}$ and $b \approx a_{bcc}$ [34]. This model accounts for the appearance of the $(^1/_2, ^1/_2, 1)_{bcc}$ major superstructure peak at about 28.2°, and is further considered as the basis for each structural model discussed below. The *Cccm* crystal structure is schematically shown in the upper left corner of Fig. 2. The results of the Rietveld analysis of the neutron diffraction pattern of our TaD sample using this model are shown in Fig. 3 and Table 1.

The coordination environment of Ta and D atoms in the *Cccm*-TaD structural model is typical of the group V transition metal hydrides with $0 < H/Me < 1$, in which H or D atoms occupy tetrahedral interstitial sites in a distorted *bcc* metal sublattice. Each deuterium atom is surrounded by a distorted tetrahedron of four Ta atoms, and each Ta atom is surrounded by four D atoms in a planar quadrilateral coordination. A comparison of the shortest interatomic distances for the currently known phases in the Ta–H(D) system is given in Table S1 in Supplementary materials.

In addition to the $(^1/_2, ^1/_2, 1)_{bcc}$ peak, we observed a series of much weaker superstructural peaks which could only be indexed assuming a $1 \times 8 \times 1$ supercell of the orthorhombic *Cccm* cell. The formation of layered superstructures based on the $1 \times 14 \times 1$, $1 \times 16 \times 1$ and $1 \times 6 \times 1$ supercells of the orthorhombic *Cccm* cell was previously observed by electron and neutron diffraction in the Nb–H(D) systems, which are a close analog of the Ta–H(D) systems, in the concentration range $0.75 < H(D)/Nb < 1$ [35,36]. Regretfully, the structural models for the H(D) ordering proposed in Refs. [35,36] cannot be regarded reliable because of the inadequate description of the structure factor in their diffraction data.

In order to reproduce the relative intensities of the minor superstructural reflections, we undertook an extended search for possible superstructure candidates. The best fit was obtained with the *P222* model shown in the middle section of Fig. 2. The key difference of this model from the structural models proposed for $NbH(D)_x$ in Refs. [35,36] is that not all shortest H–H (D-D) distances are oriented in the same direction. The corresponding fit residual is shown by the olive curve at the bottom of Fig. 3, and the refined structural parameters are listed in Table 2.

Table 2 – Structural parameters obtained from the Rietveld refinement of the NPD pattern of $TaD_{0.96}$ using the P222 (#16) model. The lattice parameters are $a = 27.783(5)$ Å, $b = 4.833(1)$ Å and $c = 4.793(1)$ Å. The refinement residual is shown by the olive curve at the bottom of Fig. 3; the reliability factors are $R_p = 3.37\%$ and $R_{wp} = 4.39\%$. The atomic thermal parameters and occupancies were assumed to be equal for all deuterium atoms. The atomic displacement parameter U_{iso} for the Ta atoms was fixed at zero, because its inclusion in the refinement did not improve the reliability factors.

Atom	Wyckoff position	x	y	z	U_{iso}, Å^2	w
Ta1	4u	25/32	3/4	3/4	0	1
Ta2	4u	27/32	3/4	1/4	0	1
Ta3	4u	29/32	3/4	3/4	0	1
Ta4	4u	31/32	3/4	1/4	0	1
Ta5	4u	9/32	3/4	3/4	0	1
Ta6	4u	11/32	3/4	1/4	0	1
Ta7	4u	13/32	3/4	3/4	0	1
Ta8	4u	15/32	3/4	1/4	0	1
D9	2k	3/4	1/2	0	0.011(1)	0.88(1)
D10	2i	3/4	0	0	0.011(1)	0.88(1)
D11	2l	13/16	1/2	1/2	0.011(1)	0.88(1)
D12	2j	13/16	0	1/2	0.011(1)	0.88(1)
D13	2k	7/8	1/2	0	0.011(1)	0.88(1)
D14	2i	7/8	0	0	0.011(1)	0.88(1)
D15	2l	15/16	1/2	1/2	0.011(1)	0.88(1)
D16	2j	15/16	0	1/2	0.011(1)	0.88(1)
D17	1c	0	1/2	0	0.011(1)	0.88(1)
D18	1a	0	0	0	0.011(1)	0.88(1)
D19	2l	5/16	1/2	1/2	0.011(1)	0.88(1)
D20	2j	5/16	0	1/2	0.011(1)	0.88(1)
D21	2k	3/8	1/2	0	0.011(1)	0.88(1)
D22	2i	7/16	0	0	0.011(1)	0.88(1)
D23	2j	7/16	0	1/2	0.011(1)	0.88(1)
D24	1h	1/2	1/2	1/2	0.011(1)	0.88(1)
D25	1e	1/2	1/2	0	0.011(1)	0.88(1)

The refinements within the *Cccm* and *P222* models were carried out with the same set of refinable parameters, which were the profile functions, instrumental parameters, background and absorption correction, atomic thermal parameters and occupancy for D atoms. The latter was refined as a free parameter because of the unknown degree of protium contamination of the deuteride. Protium impurity effectively decreases the calculated occupancy of the D atomic positions, because the coherent neutron scattering amplitude of H atoms, $b_H = -3.74$ fm, is smaller than that of D atoms, $b_D = 6.67$ fm. The atomic positions in the *P222* model were fixed so that the number of the refinable parameters was the same as in the *Cccm* model. Significant improvement in the residual *R*-factors was achieved with the *P222* model ($R_p = 3.37\%$ and $R_{wp} = 4.39\%$) as compared to the *Cccm* model ($R_p = 4.18\%$ and $R_{wp} = 5.55\%$).

When we included the atomic positions as refinable parameters in the *P222* model, these positional parameters demonstrated strong correlations, and, moreover, the residual

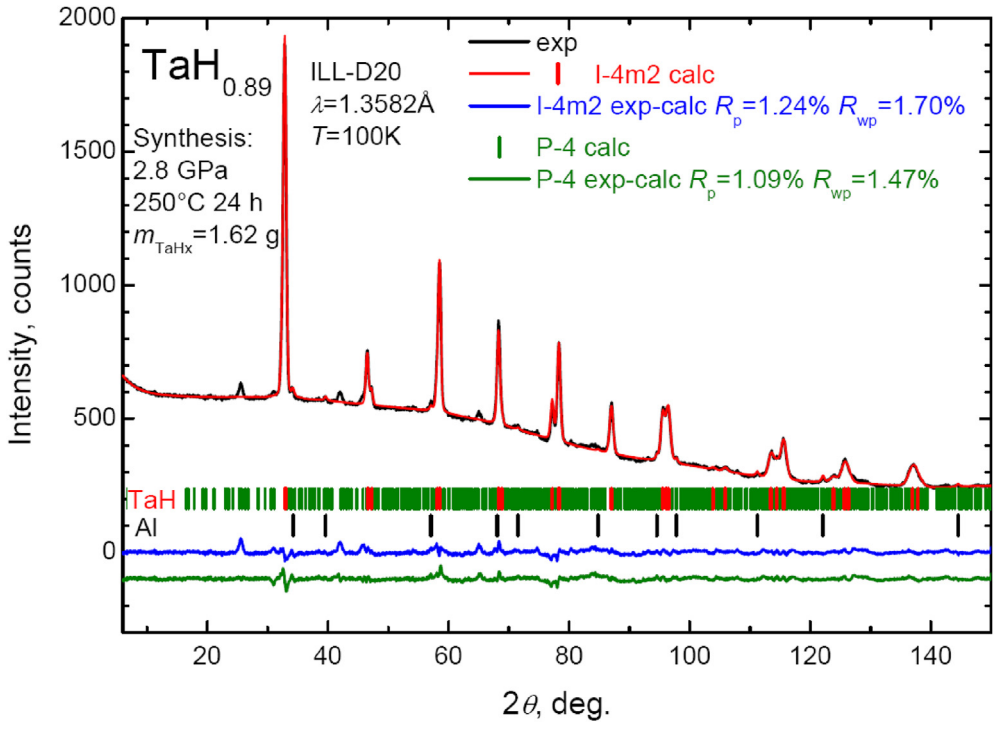

Fig. 4 – Neutron powder diffraction pattern of the $TaH_{0.89}$ sample (black curve) measured at $T = 100$ K with the D20 instrument at ILL, and the results of its Rietveld analysis using the $I\bar{4}m2$ and $P\bar{4}$ structural models. The refined structural parameters are listed in Tables 3 and 4, respectively.

Table 3 – Structural parameters obtained from the Rietveld refinement of the NPD pattern of $TaH_{0.89}$ using the $I\bar{4}m2$ (#119) model. The lattice parameters are $a = 3.405(1)$ Å and $c = 3.453(1)$ Å. The refinement residual is shown by a blue curve at the bottom of Fig. 4; the reliability factors are $R_p = 1.24\%$ and $R_{wp} = 1.70\%$.

Atom	Wyckoff position	x	y	z	U_{iso}, Å^2	w
Ta	2a	0	0	0	0.0064(2)	1
H	2d	0	1/2	3/4	0.022(1)	0.89(fixed)

R-factors did not improve significantly (R_p = 3.20% and R_{wp} = 4.10%).

The coordination environments in the *P222* and *Cccm* structural models are identical, with the exception for the Ta6 and Ta7 atoms (see Table 2), which have only 3 deuterium atoms in their first coordination spheres.

TaH

Our le Bail fits to the TaH neutron and X-ray diffraction patterns, starting with an orthorhombic unit cell, invariably converged to a tetragonal cell with $a = c$. In contrast, similar fits of the TaD patterns always showed a noticeable orthorhombic distortion of the crystal structure with a typical ratio of $(c-a)/a \approx 1\%$.

Table 4 – Structural parameters obtained from the Rietveld refinement of the NPD pattern of $TaH_{0.89}$ using the $P\bar{4}$ (#81) model. The lattice parameters are $a = 4.816(1)$ Å and $c = 24.170(5)$ Å. The refinement residual is shown by the olive curve at the bottom of Fig. 4; the reliability factors are $R_p = 1.09\%$ and $R_{wp} = 1.47\%$. The atomic thermal parameters were assumed to be equal for all atoms of the same type.

Atom	Wyckoff position	x	y	z	U_{iso}, Å^2	w
Ta1	4h	3/4	1/4	5/28	0.0076(2)	1
Ta2	4h	1/4	1/4	3/28	0.0076(2)	1
Ta3	4h	3/4	1/4	1/28	0.0076(2)	1
Ta4	4h	3/4	1/4	3/4	0.0076(2)	1
Ta5	4h	1/4	1/4	19/28	0.0076(2)	1
Ta6	4h	3/4	1/4	17/28	0.0076(2)	1
Ta7	4h	1/4	1/4	15/28	0.0076(2)	1
H8	2e	0	0	3/14	0.025(1)	1
H9	2g	0	1/2	3/14	0.025(1)	1
H10	2g	1/2	0	1/7	0.025(1)	1
H11	2f	1/2	1/2	1/7	0.025(1)	1
H12	2e	0	0	1/14	0.025(1)	1
H13	2g	0	1/2	1/14	0.025(1)	1
H14	1c	1/2	1/2	0	0.025(1)	1
H15	2g	0	1/2	5/7	0.025(1)	1
H16	2g	1/2	0	9/14	0.025(1)	1
H17	2f	1/2	1/2	9/14	0.025(1)	1
H18	2e	0	0	4/7	0.025(1)	1
H19	2g	0	1/2	4/7	0.025(1)	1
H20	1d	1/2	1/2	1/2	0.025(1)	1

It was previously reported that the high-pressure phase $TaH_{0.84}$ has a tetragonal lattice at low temperatures [24]; however, the diffraction data were not presented and the results were not conclusive. Based on electron microscopy data, it was suggested that a cubic phase with the assumed composition $TaH_{0.85}$ exists at low-temperatures [16]. It was also conjectured that a tetragonal high-concentration low-temperature phase, called γ-NbH, exists in the Nb–H system [37], but we could not find any diffraction data in the literature to support this claim. The hypothetical crystal structure of γ-NbH belongs to the space group $I\bar{4}m2$. This structure is schematically shown in the upper right corner of Fig. 2. The coordination environment of Ta atoms in this structure is slightly different from that in the *Cccm* and P222 structures discussed above. Namely, the four H atoms form a distorted tetrahedron instead of a planar quadrilateral coordination around each Ta atom.

The results of Rietveld analysis of the neutron diffraction pattern of TaH using the $I\bar{4}m2$ model are shown in Fig. 4. The obtained structural parameters are given in Table 3.

The superstructural reflections in the diffraction pattern of $TaH_{0.89}$ could not be satisfactorily indexed with the $1 \times 1 \times N$ supercells of the *bcc* unit cell; however, they could be indexed based on a $1 \times 7 \times 1$ supercell of a "doubled" ($a = c = a_{bcc}\sqrt{2}$ and $b \approx a_{bcc}$) unit cell, analogous to that of the deuteride.

Compared to $TaD_{0.96}$, the superstructural reflections in $TaH_{0.89}$ are weaker, and the pattern is less sensitive to the location of hydrogen atoms in the structure. This is due to the lower amplitude of neutron scattering by H atoms compared to D atoms and because of the anomalously large incoherent scattering of neutrons by H atoms, which inevitably increases statistical errors. Nevertheless, we attempted a search for a possible sequence of layers that would give relative intensities of the superstructural peaks similar to the experimental ones. An additional constraint was the assumption that the overall structure symmetry should be tetragonal. The best fit was obtained using the $P\bar{4}$ space group. The corresponding crystal structure is shown at the bottom of Fig. 2. The respective Rietveld refinement residual is displayed by the olive curve at the bottom of Fig. 4. The refined atomic parameters are listed in Table 4 below.

With the number of refinable parameters being the same in both models, one can see a substantial improvement of the reliability factors in the $P\bar{4}$ model ($R_p = 1.09\%$ and $R_{wp} = 1.47\%$) over the $I\bar{4}m2$ model ($R_p = 1.24\%$ and $R_{wp} = 1.70\%$). It was not possible to refine the atomic positional parameters for the $P\bar{4}$ model because these parameters were strongly correlated.

The coordination environments in the $P\bar{4}$ and P222 structures are similar. In the $P\bar{4}$ structure there are four atoms – Ta3, Ta4, Ta5, and Ta7 – which have only three nearest-neighbor H atoms (see Table 4).

Inelastic neutron scattering

INS spectra, or dynamical structure factors *S*(*E*), of TaH and TaD collected with the IN1-Lagrange spectrometer are shown at the top and bottom of Fig. 5 by the black and red curves, respectively.

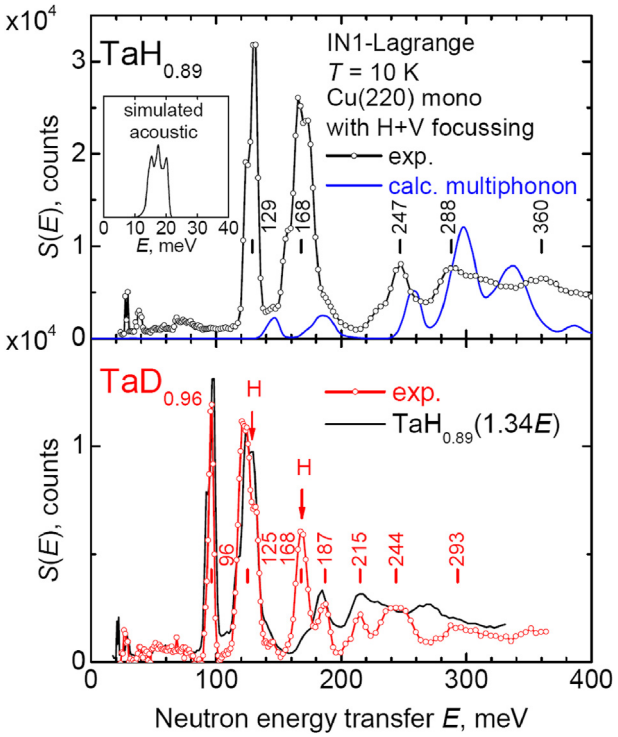

Fig. 5 – Top: the dynamical structure factor *S*(*E*) of the $TaH_{0.89}$ sample as a function of the neutron energy loss *E* (black curve). The vertical ticks show the positions of the experimental peaks. The blue curve shows a simulated multiphonon contribution, calculated in a harmonic isotropic approximation. The inset shows a simulated acoustic vibrational part, which was later used for multiphonon calculation. Bottom: *S*(*E*) for the $TaD_{0.96}$ sample (red curve), experimental peak positions (red ticks with numbers) and the INS spectrum of $TaH_{0.89}$ from the top panel, scaled down by a factor of 1.34 along the energy axis (black curve). The peaks marked with "H" are the local (defect) modes of protium impurity. The spurious intensity below 90 meV results from the little account of inelastic scattering in the beryllium filter and a minor contamination of the incoming neutron beam with λ/2-neutrons. (For interpretation of the references to color in this figure legend, the reader is referred to the Web version of this article.)

The fundamental band of hydrogen vibrations in TaH consists of two peaks. The peak at 129 meV corresponds to a vibration in the direction to the nearest O-site, which is along the z-axis of the $I\bar{4}m2$ structure, and the peak at 168 meV is caused by a double degenerate vibration in the perpendicular plane. In the INS spectrum of the deuteride, the peaks are located at 96 and 125 meV, respectively. For brevity, these vibrational states will be labeled as H(D)|z and H(D)|x,y, respectively.

All scattering intensity for $S_{TaH}(E)$ at $E > E_{max} = 200$ meV results from multiphonon processes. To estimate the anharmonicity of H vibrations in TaH, we simulated the multiphonon scattering in the harmonic isotropic approximation

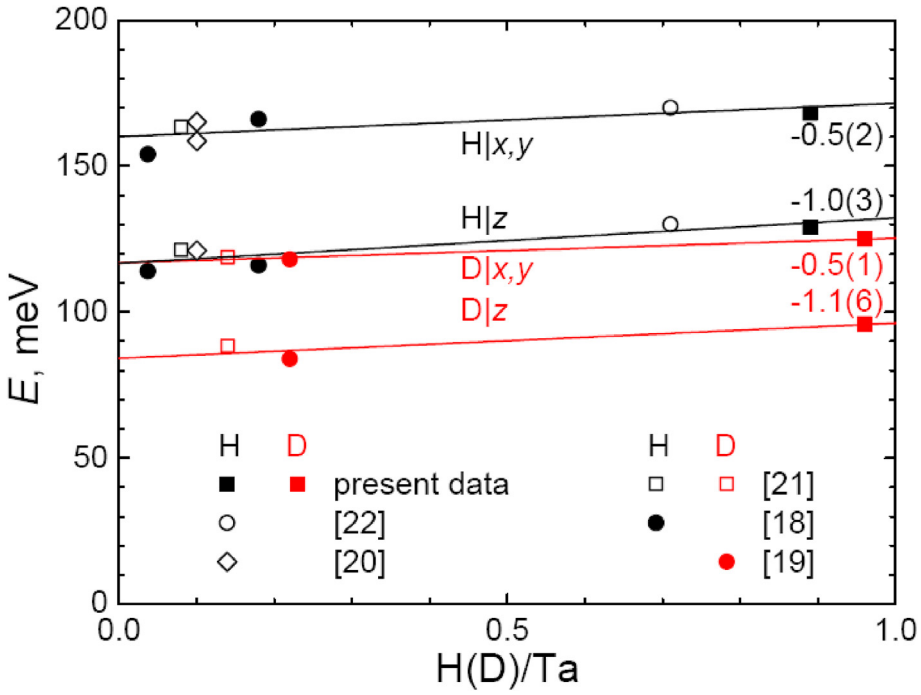

Fig. 6 – Dependences of the fundamental vibrational energies in TaH_x (black symbols) and TaD_x (red symbols) on the H(D)/Ta ratios. Results of the present paper are shown by the filled squares; other symbols stand for the literature data. The lines are the guides for the eye. The numbers indicate the Grüneisen parameters $\gamma = -\frac{V}{E}\frac{dE}{dV}$ calculated assuming dV/d(H(D)/Ta) = 2.4 Å^3/H(D) atom [25]. (For interpretation of the references to color in this figure legend, the reader is referred to the Web version of this article.)

using an iterative technique [38]. For this, it was necessary to know the distribution of the INS intensity over the entire energy range from $E = 0$ to the maximum single-phonon energy E_{max}. We removed the spurious contribution from the λ/2 neutrons at $E < 110$ meV and complemented the optical part of $S_{TaH}(E)$, measured experimentally, with a simulated and properly normalized acoustic part, using a procedure similar to that in Ref. [7]. The resulting simulated multiphonon contribution to $S_{TaH}(E)$ is shown by the blue curve in Fig. 5. It is important to note that our multiphonon simulation is free from any model-dependent parameters and fits.

As one can see from Fig. 5, the agreement between the experimental $S_{TaH}(E)$ and simulated multiphonon contribution at $E > E_{max}$ is very poor. Particularly, a two-phonon process 2 × H|z appears at 247 meV instead of 2 × 129 = 258 meV, expected in the harmonic approximation, and a H|z × H|x,y process occurs at 288 meV instead of 129 + 168 = 297 meV. This clearly indicates a strong "soft", or "trumpet-like", anharmonicity of the potential well for the hydrogen atom. This conclusion is consistent with previous INS results for $TaH_{0.71}$ [22].

The $S_{TaH}(E)$ spectrum at $E > 300$ meV looks like a rather featureless background, and it is difficult to attribute a wide hump at ~360 meV to a specific multiphonon process, for example, 2 × H|x,y or 3 × H|z.

Although we were unable to perform multiphonon simulations for TaD due to the uncertainties in subtracting the protium contamination, it is clear that the potential well for the D atom also demonstrates "soft" anharmonicity. However, the anharmonicity in the two-phonon vibrational band of TaD is less pronounced in comparison to TaH: the experimental peak positions at 187, 215 and 244 meV are within 5–6 meV from the energies of the, respectively, 2 × H|z, H|z × H|x,y, and 2 × H|x,y processes estimated in the harmonic approximation. This is a manifestation of the proximity of the potential well to the harmonic form near the bottom of the well, where D atoms have higher probability to be found than H atoms.

The protium contamination of our sample of tantalum deuteride can be estimated as H/(D + H) = 0.054, based on the intensity of the local (defect) mode of hydrogen vibrations at 168 meV. This significant enrichment in protium compared to H/(D + H) = 0.015 in AlD_3 used as the internal deuterium source in the high-pressure cell indicates that the isotopic separation factor $(H/D)_{hydride}/(H/D)_{gas}$ is above unity for the Ta–H(D) system. The contamination with protium leads to a decrease in the calculated occupation factor for D-sites in diffraction experiments by $w_{eff} = 1 + \frac{H}{D+H}\left(\frac{b_H}{b_D} - 1\right) = 0.92$, which is reasonably close to the refined value of $w = 0.88$ in the P222 structural model for TaD (see Section TaD).

In many transition metal-hydrogen systems, such as Pd–H [39], the position of the fundamental peak of H vibrations shifts significantly towards lower energies as the H/Me concentration increases, which is a result of the weakening of the H–Me interaction caused by the lattice expansion. In the Ta–H(D) system, the situation is reversed, as can be seen from the E(H(D)/Ta) dependencies shown in Fig. 6. The Grüneisen parameters of both optical modes, defined as $\gamma = -\frac{V}{E}\frac{dE}{dV}$, are negative.

Except for the local (defect) H-impurity mode at 168 meV, the fundamental region of the $S(E)$ spectrum of TaD can be reasonably well approximated by that of TaH, if the latter is scaled down by a factor of 1.34 along the energy axis. The large deviation of this E_H/E_D scaling factor from its harmonic value $\sqrt{2} = 1.41$ is due to two effects – differences in the crystal structures of TaH and TaD and "soft" anharmonicity.

Previous INS studies of diluted solutions of H and D in Ta [21] gave the energy scaling factor $E_H/E_D = 1.38$, which was attributed solely to the anharmonicity. One can expect that the anharmonicity, like the fundamental vibrational frequency, weakly depends on the H(D)/Ta ratio, because the potential well for the H(D) atom is mostly determined by the surrounding metal atoms, and not by the neighboring H(D) atoms in the second and higher coordination spheres. Most likely, the significantly lower experimental value of $E_H/E_D = 1.34$ for TaH and TaD obtained in the present work cannot be explained by the anharmonicity alone.

On the one hand, the shortest H–Ta distances in the $P\bar{4}$ structural model, r(H–Ta) = 1.909 Å, are nearly identical to the shortest D-Ta distances in the $P222$ structural model, r(D-Ta) = 1.910 Å, assuming that the H and D atoms are situated at the centers of the tetrahedral interstices. Thus, if we imagine a hypothetical $P222$ crystal structure, in which deuterium is substituted with protium, one could expect that the difference in the vibrational properties between the $P\bar{4}$ and hypothetical $P222$ hydrides should be negligible. On the other hand, the fact that the ground state crystal structures of TaH and TaD are different can only be ascribed to the zero-point energy (ZPE) contribution to the formation enthalpy of these phases. If we assume that two different TaH phases — $P\bar{4}$ and hypothetical $P222$ — have the same phonon density of states $g(E)$ (or, equivalently, the same $S(E)$), the ZPE contribution to the formation enthalpy of these phases, which is $E_{ZPE} = \frac{3}{2}\int_0^{E_{max}} Eg(E)dE / \int_0^{E_{max}} g(E)dE$, will also be the same.

The ZPE contributions to the formation enthalpies of the corresponding TaD phases will also be the same, and the inclusion of ZPE will not change the relative stabilities of the $P\bar{4}$ and $P222$ phases when H is substituted by D. Since this contradicts the observations in our case, we can conclude that $S(E)$ for the $P\bar{4}$-TaH and for the hypothetical $P222$–TaH should be significantly different, and this should substantially affect the scaling factor E_H/E_D discussed above.

Conclusions

In this work, we synthesized massive samples of tantalum monohydride $TaH_{0.89}$ and monodeuteride $TaD_{0.96}$ under high hydrogen (deuterium) pressures and studied them at ambient pressure with neutron diffraction and inelastic neutron scattering. The compositions of the obtained samples correspond to the maximal achievable saturation of *bcc* tantalum with H(D) before it transforms into *hcp* dihydride.

Surprisingly, the hydrogen and deuterium arrangement in the crystal structures of our samples turned out to be different. The hydrogen atoms in $TaH_{0.89}$ are ordered within a $\sqrt{2} \times \sqrt{2} \times 7$ supercell of the initial *bcc* unit cell (space group $P\bar{4}$, see Table 4), whereas the deuterium atoms in $TaD_{0.96}$ are ordered within a $\sqrt{2} \times \sqrt{2} \times 8$ supercell (space group $P222$, see Table 2). This very rare phenomenon was previously observed only in the V–H(D) [9,10] and La–H(D) [5] systems.

Inelastic neutron scattering demonstrated that the potential well for the H(D) atom in TaH(D) has a pronounced trumpet-like anharmonicity – the higher the energy, the smaller the distance between successive vibrational energy levels. A similar anharmonicity was earlier observed in low concentration Ta–H and Ta-D samples [21]. The stabilization of different crystal structures for the hydride and deuteride with almost the same H/Ta and D/Ta ratios is the result of different contribution to the formation enthalpies of these phases from their different vibrational properties.

Presently available theoretical calculations for the Ta–H system [17] did not take into account compounds with $0 < H(D)/Ta < 1$, which are stable at low H_2 pressures. Our results demonstrate that proper consideration of the zero-point energy and anharmonicity of hydrogen vibrations, as well as the non-stoichiometric composition of the phase, can be critically important for correct predictions of the crystal structures of the ground state of metal hydrides from *ab initio* calculations.

Declaration of competing interest

The authors declare that they have no known competing financial interests or personal relationships that could have appeared to influence the work reported in this paper.

Acknowledgments

The work was partly supported by the Russian Foundation for Basic Research [grant No. 20-02-00638]. A.I.K. acknowledges the support by the Scientific User Facilities Division, Office of Basic Energy Sciences, US Department of Energy.

Appendix A. Supplementary data

Supplementary data to this article can be found online at https://doi.org/10.1016/j.ijhydene.2021.03.149.

REFERENCES

[1] Drozdov AP, Eremets MI, Troyan IA, Ksenofontov V, Shylin SI. Conventional superconductivity at 203 kelvin at high pressures in the sulfur hydride system. Nature 2015;525:73–6. https://doi.org/10.1038/nature14964.

[2] Einaga M, Sakata M, Ishikawa T, Shimizu K, Eremets MI, Drozdov AP, Troyan IA, Hirao N, Ohishi Y. Crystal structure of the superconducting phase of sulfur hydride. Nat Phys 2016;12:835–8. https://doi.org/10.1038/nphys3760.

[3] Troyan IA, Semenok DV, Kvashnin AG, Sadakov AV, Sobolevskiy OA, Pudalov VM, Ivanova AG, Prakapenka VB, Greenberg E, Gavriliuk AG, Struzhkin VV, Bergara A, Errea I, Bianco R, Calandra M, Mauri F, Monacelli L, Akashi R,

Oganov AR. Anomalous high-temperature superconductivity in YH_6. Adv Mater 2021:2006832. https://doi.org/10.1002/adma.202006832.
[4] Kong PP, Minkov VS, Kuzovnikov MA, Besedin SP, Drozdov AP, Mozaffari S, Balicas L, Balakirev FF, Prakapenka VB, Greenberg E, Knyazev DA, Eremets MI. Superconductivity up to 243 K in yttrium hydrides under high pressure. 2019. arXiv:1909.10482.
[5] Drozdov AP, Kong PP, Minkov VS, Besedin SP, Kuzovnikov MA, Mozaffari S, Balicas L, Balakirev F, Graf D, Prakapenka VB, Greenberg E, Knyazev DA, Tkacz M, Eremets MI. Superconductivity at 250 K in lanthanum hydride under high pressures. Nature 2019;569:528–31. https://doi.org/10.1038/s41586-019-1201-8.
[6] Somayazulu M, Ahart M, Mishra AK, Geballe ZM, Baldini M, Meng Y, Struzhkin VV, Hemley RJ. Evidence for superconductivity above 260 K in lanthanum superhydride at megabar pressures. Phys Rev Lett 2019;122:027001. https://doi.org/10.1103/PhysRevLett.122.027001.
[7] Kuzovnikov MA, Antonov VE, Ivanov AS, Hansen T, Savvin S, Kulakov VI, Tkacz M, Kolesnikov AI, Gurev VM. Neutron scattering study of tantalum dihydride. Phys Rev B 2020;102:024113. https://doi.org/10.1103/PhysRevB.102.024113.
[8] San-Martin A, Manchester FD. The H-Ta (Hydrogen-Tantalum) system. J Phase Equil 1991;12:332–43. https://doi.org/10.1007/BF02649922.
[9] Schober T. Vanadium-, niobium- and tantalum-hydrogen. In: Lewis FA, Aladjem A, editors. Solid state phenomena, 49–50. Trans Tech Publications; 1996. p. 357–422.
[10] Pesch W, Schober T, Wenzl H. A TEM study of the phase diagrams VH and VD. Scripta Metall 1982;16:307–12. https://doi.org/10.1016/0036-9748(82)90358-1.
[11] Petrunin VF, Somenkov VA, Shilshtein SS, Chertkov AA. Sov Phys-Crystallogr 1970;15:137–9 (Kristallografia 15, 171-173 (1970), in Russian).
[12] Hirabayashi M, Asano H. Order-disorder phenomena in metal hydrides. In: Bambakidis G, editor. Metal hydrides. New York: Plenum Press; 1981. p. 53–80.
[13] Somenkov VA, Chervyakov AY, Shilstein SS, Chertkov AA. Sov Phys-Crystallogr 1972;17:274–80 (Kristallografia 17 (1972) 323-327, in Russian).
[14] Somenkov VA. Structure of hydrides. Ber. Bunsenges. Phys. Chem. 1972;76(8):733–40. https://doi.org/10.1002/bbpc.19720760807.
[15] Köbler U, Schober T. Susceptibility and phase diagram of the Ta-H system. J Less Common Met 1978;60:101–7. https://doi.org/10.1016/0022-5088(78)90094-2.
[16] Schober T. Electron microscopy of niobium and tantalum hydrides. In: Proc. 9th international congress on electron microscopy, Toronto. 1; 1978. p. 644–5.
[17] Zhuang Q, Jin X, Cui T, Ma Y, Lv Q, Li Y, Zhang H, Meng X, Bao K. Pressure-stabilized superconductive ionic tantalum hydrides. Inorg Chem 2017;56:3901–8. https://doi.org/10.1021/acs.inorgchem.6b02822.
[18] Magerl A, Rush JJ, Rowe JM. Local modes in dilute metal-hydrogen alloys. Phys Rev B 1986;33:2093–7. https://doi.org/10.1103/PhysRevB.33.2093.
[19] Magerl A, Stump N, Teuchert WD, Wagner V, Alefeld G. Phonons in Ta-D and Ta-H alloys. J Phys C: Solid State Phys 1977;10:2783–9. https://doi.org/10.1088/0022-3719/10/15/014.
[20] Ikeda S, Watanabe N. Local modes and hydrogen potentials in metal hydrides. J. Phys Soc. Japan 1987;56:565–76. https://doi.org/10.1143/JPSJ.56.565.
[21] Hempelmann R, Richter D. Localized vibrations of H and D in Ta and their relation to the H(D) potential. Z Phys B: Condens Matter 1981;44:159–65. https://doi.org/10.1007/BF01297171.
[22] Eckert J, Goldstone JA, Tonks D, Richter D. Inelastic neutron scattering studies of vibrational excitations of hydrogen in Nb and Ta. Phys Rev B 1983;27:1980–90. https://doi.org/10.1103/PhysRevB.27.1980.
[23] Liu G, Besedin S, Irodova A, Liu H, Gao G, Eremets M, Wang X, Ma Y. Nb-H system at high pressures and temperatures. Phys Rev B 2017;95:104110. https://doi.org/10.1103/PhysRevB.95.104110.
[24] Szafrański AW, Tkacz M, Majchrzak S, Züchner H. Resistometric studies of the Ta-H system at high pressures and low temperatures. J Less Common Met 1984;101:523–7. https://doi.org/10.1016/0022-5088(84)90127-9.
[25] Kuzovnikov MA, Tkacz M, Meng H, Kapustin DI, Kulakov VI. High-pressure synthesis of tantalum dihydride. Phys Rev B 2017;96:134120. https://doi.org/10.1103/PhysRevB.96.134120.
[26] Ying J, Li X, Greenberg E, Prakapenka VB, Liu H, Struzhkin VV. Synthesis and stability of tantalum hydride at high pressures. Phys Rev B 2019;99:224504. https://doi.org/10.1103/PhysRevB.99.224504.
[27] Khvostantsev LG, Slesarev VN, Brazhkin VV. Toroid type high-pressure device: history and prospects. High Pres Res 2004;24:371–83. https://doi.org/10.1080/08957950412331298761.
[28] Antonov VE. Phase transformations, crystal and magnetic structures of high-pressure hydrides of d-metals. J Alloys Compd 2002;330–332:110–6. https://doi.org/10.1016/S0925-8388(01)01532-8.
[29] Hansen TC, Henry PF, Fischer HE, Torregrossa J, Convert P. The D20 instrument at the ILL: a versatile high-intensity two-axis neutron diffractometer. Meas Sci Technol 2008;19:034001. https://doi.org/10.1088/0957-0233/19/3/034001.
[30] Kuzovnikov M, Ivanov A, Savvin S, Tkacz M. Crystal structure of novel tantalum hydrides. Institut Laue-Langevin (ILL); 2019. https://doi.org/10.5291/ILL-DATA.5-22-769.
[31] Rodríguez-Carvajal J. Recent advances in magnetic structure determination by neutron powder diffraction. Phys B Condens Matter 1993;192:55–69. https://doi.org/10.1016/0921-4526(93)90108-I.
[32] Ivanov A, Jiménez-Ruiz M, Kulda J. IN1-Lagrange - the new ILL instrument to explore vibration dynamics of complex materials. J Phys: Conf. Ser. 2014;554:012001. https://doi.org/10.1088/1742-6596/554/1/012001.
[33] Kuzovnikov M, Ivanov A, Tkacz M. Vibrational dynamics of novel tantalum hydrides. Institut Laue-Langevin (ILL); 2019. https://doi.org/10.5291/ILL-DATA.7-01-487.dataset.
[34] Somenkov VA, Gurskaya AV, Zemlyanov MG, Kost ME, Chernoplekov NA, Chertkov AA. Sov Phys Solid State 1969;10(9):2123 (Fizika Tverdogo Tela 10(9) (1968) 2697-2703, in Russian).
[35] Brun TO, Kajitani T, Mueller MH, Westlake PG, Makenas BJ, Birnbaum HK. The structure of the λ-phase of niobium-deuterium. In: Proceedings of the modulated structures meeting, Kailua-Kona, AIP Conf. Proc. 53; 1979. p. 397–9. https://doi.org/10.1063/1.31811.
[36] Makenas BJ, Birnbaum HK. Phase changes in the niobium-hydrogen system-II. Low temperature hydride phase transitions. Acta Metall 1982;30:469–81. https://doi.org/10.1016/0001-6160(82)90227-9.
[37] Hauck J. Ordering of hydrogen in niobium hydride phases. Acta Crystallogr 1977;A33:208. https://doi.org/10.1107/S0567739477000424.
[38] Antonov VE, Belash IT, Kolesnikov AI, Mayer J, Natkaniec I, Ponyatovskii EG, Fedotov VK. Neutron scattering study of the vibrational spectrum of manganese hydride. Sov Phys Solid State 1991;33:87–90 (Fiz. Tverd. Tela (Leningrad) 33 (1991) 152-157, in Russian).
[39] Rush JJ, Rowe JM, Richter D. Direct determination of the anharmonic vibrational potential for H in Pd. Z Phys B Condens Matter 1984;55:283–6. https://doi.org/10.1007/BF01304078.